
Second-Order Fine-Tuning without Pain for LLMs: A Hessian Informed Zeroth-Order Optimizer

Yanjun Zhao^{1,*}Sizhe Dang^{1,*}Haishan Ye^{1,†}Guang Dai²Yi Qian¹Ivor W.Tsang³¹ Xi'an Jiaotong University, China ² SGIT AI Lab, Xi'an, China³ Centre for Frontier Artificial Intelligence Research, A* STAR, Singapore

Abstract

Fine-tuning large language models (LLMs) is necessary for specific downstream tasks, but the classic adaptive first-order optimizer entails prohibitive GPU memory because of backpropagation. Recent works such as MeZO have turned to zeroth-order optimizers for fine-tuning, which reduce substantial memory by using just two forward passes. However, heterogeneous curvatures across different parameter dimensions in LLMs often cause convergence instability or even failure. In this work, we propose HiZOO, a diagonal **Hessian informed Zeroth-Order Optimizer**, which is the first to leverage the diagonal Hessian to enhance ZOO for fine-tuning LLMs. We provide the theoretical proof for HiZOO and visualize the optimization trajectories on the test functions. Extensive experiments on various models (RoBERTa, OPT, Phi-2, and LLama3, with 350M~66B parameters) indicate that HiZOO significantly reduces the number of training steps and improves model accuracy. For example, on the SST2 task, HiZOO achieves an **8x** speed-up and better accuracy. Even when scaled to 66B-model, HiZOO outperforms MeZO with up to **5.1%** absolute improvement. We also propose HiZOO-L, which reduces the Hessian memory cost to **10%** of the MeZO, while maintaining almost same performance. Compared with ZO-Adam, HiZOO-L achieves a **4.3%** absolute improvement, just using **50%** of the GPU memory. Code is available at <https://anonymous.4open.science/r/HiZOO-27F8>.

1 Introduction

Fine-tuning pre-trained large language models (LLMs) for specific tasks has garnered significant attention. As the number of model parameter increases, full parameter fine-tuning (FT) becomes markedly memory-intensive. To alleviate the memory limitations, Parameter Efficient Fine-Tuning (PEFT) methods [19, 24, 10, 60, 35] have been developed, which only fine-tune a small number of (extra) model parameters. As a result, they significantly reduce computational and storage costs, while achieving performance comparable to a fully fine-tuned model.

First-order optimizers such as Adam [22] and AdamW [29] are widely used to fine-tune LLMs. Nevertheless, using these optimizers still leads to substantial memory consumption, primarily due to the inherent backpropagation process. To address these limitations, MeZO [32] proposed to utilize a zeroth-order optimizer (ZOO) to estimate the gradient with just two forward passes per step, no need

* Equal contribution. † Correspondence to: yehaishan@xjtu.edu.cn

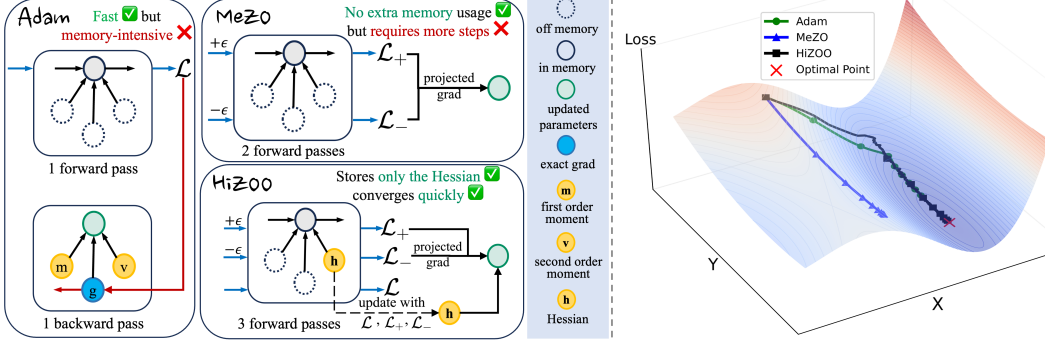


Figure 1: (Left) Comparison of HiZOO, MeZO and Adam. (Right) The test example with heterogeneous curvatures. HiZOO updates along the direction with greater curvature (X) and converges more quickly than MeZO. The corresponding loss curves are shown in Section 3.5.

for backpropagation anymore. This achieves numerous memory reduction and makes it accessible to train and store LLMs on consumer hardware.

However, parameters of LLMs often exhibit heterogeneous curvatures across different dimensions, as documented in recent studies [39, 16, 55]. This significant difference in curvature would make model converge towards the saddle point, slowing down the convergence speed, as shown in Figure 1 (right). Since the incorporation of Hessian to measure the curvature properties of the loss landscape, second order methods [26, 50, 2] can solve this sub-optimal behaviour. Unfortunately, in the context of zeroth-order optimization, one cannot directly compute the Hessian atop first-order derivatives.

In light of above, we propose HiZOO, as shown in Figure 1 (left), which estimates the diagonal Hessian by one more forward pass. HiZOO can act as a pre-conditioner, directly adjusting the update size of different parameters according to their curvatures. So that it can improve the model convergence when encountered with heterogeneous curvatures. As shown in Figure 2, HiZOO can significantly reduce the training steps and improve the accuracy. Here we summarize our key contributions as follows:

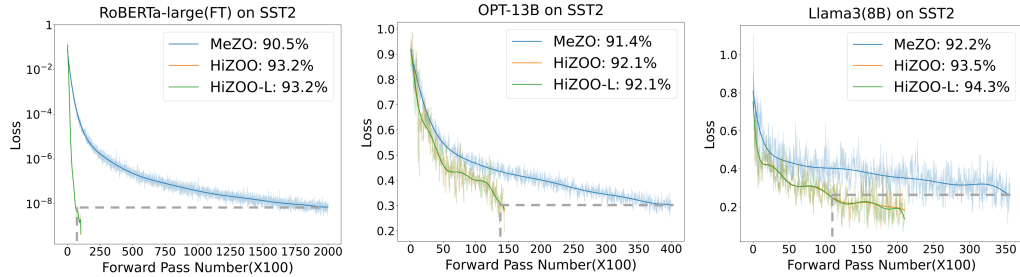


Figure 2: Performance of MeZO, HiZOO and HiZOO-L on SST2 task, when fine-tuning RoBERTa-large, OPT-13B, Llama3(8B) models. HiZOO can achieve 8 \times speedup and 1.55% absolute accuracy improvement compared with MeZO. Experiments are conducted with the same learning rate.

1. In this work, we estimate the Hessian in zeroth-order optimizer to fine-tune LLMs for the first time. Our HiZOO reduces the total number of forward passes required for model convergence and achieves better accuracy. By utilizing diagonal Hessian, HiZOO reduces the corresponding memory cost from $\mathcal{O}(d^2)$ to $\mathcal{O}(d)$. Furthermore, we propose HiZOO-L, reducing the memory usage of Hessian to **10%** of the MeZO.
2. We provide theoretical analysis to prove that HiZOO provides an unbiased estimation of the Hessian. Also, we illustrate how HiZOO utilizes Hessian to improve the convergence process by visualizing the optimization trajectories on test functions.
3. We conduct extensive experiments across different models (RoBERTa-large, OPT, Llama3 and Phi-2) with scales from 350M to 66B, different methods (FT, LoRA, prefix), and different downstream tasks (classification, multiple-choice, and generation) to verify the effect of the HiZOO. For example, on SST2 task HiZOO achieves a 1.55% accuracy improvement and

$8\times$ speedup over MeZO on average across different models. Even on OPT-66B, HiZOO outperforms better than MeZO with up to 5% improvement.

4. Further exploration in Section 4.3 showcases that HiZOO can achieve better performance in optimizing non-differentiable objectives such as F1 score. Specifically, HiZOO significantly outperforms the MeZO’s results with 6.5% on average.

2 Related Works

Here we present a concise overview on optimizers used in fine-tuning LLMs(details in Appendix A).

First-Order Optimizer in LLMs First-order optimizers, such as Gradient Descent (GD), Momentum, Adagrad [12], are fundamental in many areas like computer vision, natural language processing (NLP). Among them, Adam [22] plays a dominant role due to its fast convergence and is often chosen for training and fine-tuning LLMs. AdamW [29] improves upon Adam by adding the weight decay to alleviate overfitting. But both of them requires lots of memory cost due to the backpropagation process.

First-Order Optimizer Enhanced with Hessian On the other hand, researchers incorporated second-order information (Hessian) to provide richer guidance for gradient descent during the training. For example BROYDEN [4], Nesterov & Polyak [34] and Conn et al. [7] utilized curvature information to pre-condition the gradient; Magoulas et al. [31] applied diagonal Hessian as the pre-conditioner; Martens [33] approximated the Hessian with conjugate gradient. Sophia [26] used a light-weight estimate of the diagonal Hessian for pre-training LLMs. Despite their potential, above optimizers require the enormous GPU-memory cost.

Zeroth-Order Optimizer Zeroth-order optimizers, with just forward passes, can greatly reduce the memory consumption. Methods like SPSA [42] have been shown to perform well in non-convex multi-agent optimization [44, 18] or generating black-box adversarial examples [6, 5, 27, 52]. Recently, MeZO [32] firstly adapted the classical ZO-SGD method to fine-tune LLMs, achieving comparable performance with significant memory reduction. But these methods often struggle with heterogeneous curvatures.

3 Methods

In the following, we briefly introduce the classical ZO gradient estimator SPSA [42], which is used in MeZO. Then we describe how HiZOO estimates diagonal Hessian and cooperates with ZOO.

3.1 Preliminaries

Definition 3.1. (Simultaneous Perturbation Stochastic Approximation or SPSA). Given a model with parameters $\theta \in \mathbb{R}^d$ and loss function \mathcal{L} , SPSA estimates the gradient on a minibatch \mathcal{B} as:

$$g'_\mu(\theta_t) = \frac{\mathcal{L}(\theta_t + \mu u; \mathcal{B}) - \mathcal{L}(\theta_t - \mu u; \mathcal{B})}{2\mu} u \approx u u^\top \nabla \mathcal{L}(\theta_t; \mathcal{B}),$$

where $u \in \mathbb{R}^d$ and is sampled from $\mathcal{N}(0, I_d)$, μ is the *perturbation scale*. The n -SPSA gradient estimate averages $g_\mu(\theta)$ over n randomly sampled u .

3.2 Hessian Informed Zeroth-Order Optimization

We will present how to estimate Hessian inverse matrix Σ in detail in Section 3.3. Given Σ , then we can construct the following descent direction:

$$g_\mu(\theta_t) = \sum_{i=1}^n \frac{\mathcal{L}(\theta_t + \mu \Sigma_t^{1/2} u_i; \mathcal{B}) - \mathcal{L}(\theta_t - \mu \Sigma_t^{1/2} u_i; \mathcal{B})}{2\mu \cdot n} \cdot \Sigma_t^{1/2} u_i. \quad (1)$$

With the above descent direction, we can update θ_t as follows:

Algorithm 1 HiZOO

Require: parameters $\theta \in \mathbb{R}^d$, loss $L : \mathbb{R}^d \rightarrow \mathbb{R}$, step budget T , perturbation scale μ , learning rate schedule η_t , smooth scale α_t , diagonal Hessian Σ_0

- 1: **for** $t = 1, \dots, T$ **do**
- 2: Sample batch $\mathcal{B} \subset \mathcal{D}$ and random seed s
- 3: $\ell \leftarrow \mathcal{L}(\theta; \mathcal{B})$
- 4: $\theta \leftarrow \text{PerturbParameters}(\theta, \mu, \Sigma_{t-1}^{1/2}, s)$
- 5: $\ell_+ \leftarrow \mathcal{L}(\theta; \mathcal{B})$
- 6: $\theta \leftarrow \text{PerturbParameters}(\theta, -2\mu, \Sigma_{t-1}^{1/2}, s)$
- 7: $\ell_- \leftarrow \mathcal{L}(\theta; \mathcal{B})$
- 8: $\theta \leftarrow \text{PerturbParameters}(\theta, \mu, \Sigma_{t-1}^{1/2}, s)$ ▷ Reset parameters before descent
- 9: $\Sigma'_t = \frac{1}{2\mu^2}(\ell_+ + \ell_- - 2\ell)(\Sigma_{t-1}^{-1/2}u_i u_i^\top \Sigma_{t-1}^{-1/2})$ ▷ Update diagonal Hessian
- 10: $\Sigma_t^{-1} = (1 - \alpha_t)\Sigma_{t-1}^{-1} + \alpha_t |\text{diag}(\Sigma'_t)|$
- 11: projected_grad $\leftarrow (\ell_+ - \ell_-) * \Sigma_t^{1/2} / 2\mu$
- 12: Reset random number generator with seed s ▷ For sampling u_i
- 13: **for** $\theta_i \in \theta$ **do**
- 14: Sample $u_i \sim \mathcal{N}(0, I_d)$
- 15: $\theta_i \leftarrow \theta_i - \eta_t * \text{projected_grad} * u_i$
- 16: **end for**
- 17: **end for**
- 18: **function** PERTURBPARAMETER($\theta, \mu, \Sigma_t^{1/2}, s$)
- 19: Reset random number generator with seed s ▷ For sampling u_i
- 20: **for** $\theta_i \in \theta$ **do**
- 21: Sample $u_i \sim \mathcal{N}(0, I_d)$
- 22: $\theta_i \leftarrow \theta_i + \mu \Sigma_t^{1/2} u_i$ ▷ Modify parameters in place
- 23: **end for**
- 24: **return** θ
- 25: **end function**

$$\theta_{t+1} = \theta_t - \eta_t g_\mu(\theta_t). \quad (2)$$

It's guaranteed that $g_\mu(\theta)$ can estimate the descent direction by the following equation:

$$\begin{aligned} \mathbb{E}[\mathcal{L}(\theta_{t+1}; \mathcal{B})] &= \mathcal{L}(\theta_t; \mathcal{B}) - \eta_t \mathbb{E}[\langle \nabla \mathcal{L}(\theta_t; \mathcal{B}), g_\mu(\theta_t) \rangle] + \mathcal{O}(\eta_t^2) \\ &= \mathcal{L}(\theta_t; \mathcal{B}) - \eta_t \frac{1}{b} \mathbb{E} \left[\sum_{i=1}^b \langle \nabla \mathcal{L}(\theta_t; \mathcal{B}), \Sigma_t^{1/2} u_i u_i^\top \Sigma_t^{1/2} \nabla \mathcal{L}(\theta_t; \mathcal{B}) \rangle \right] + \mathcal{O}(\eta_t^2) + \mathcal{O}(\mu) \\ &= \mathcal{L}(\theta_t; \mathcal{B}) - \eta_t \|\Sigma_t^{1/2} \nabla \mathcal{L}(\theta_t; \mathcal{B})\|^2 + \mathcal{O}(\eta_t^2) + \mu, \end{aligned}$$

where the first and second equality are both from the Taylor's expansion. Above equation shows that when η_t is properly chosen, $g_\mu(\theta)$ can accurately estimate the direction of gradient descent, which is the key to the success of fine-tuning large language models.

3.3 Diagonal Hessian Estimator

Storing the exact full spectral Hessian ($d \times d$) requires $\mathcal{O}(d^2)$ memory [49, 48, 9], which is sufficient but never necessary. In HiZOO, we just estimate and retain only the diagonal Hessian which requires $\mathcal{O}(d)$ memory. It serves as a pre-conditioner to scale the direction and magnitude of the model parameter updates according to their respective curvatures.

Drawing from the lemma presented in MiNES [51]:

$$\frac{1}{2} \cdot \mathbb{E}_u(u^\top \Sigma^{1/2} H \Sigma^{1/2} u \cdot (\Sigma^{-1/2} u u^\top \Sigma^{-1/2} - \Sigma^{-1})) = H, \quad (3)$$

where H is the Hessian $\nabla^2 \mathcal{L}(\theta; \mathcal{B})$ and Σ is a positive definite matrix with $\Sigma^{-1} \approx \nabla^2 \mathcal{L}(\theta; \mathcal{B})$.

Thus, we can approximate the diagonal Hessian by the zeroth order oracles. Firstly, we will access to the $\mathcal{L}(\theta + \mu \Sigma^{1/2} u; \mathcal{B})$, $\mathcal{L}(\theta - \mu \Sigma^{1/2} u; \mathcal{B})$ and $\mathcal{L}(\theta; \mathcal{B})$. Through the Taylor's expansion, we yield the following results:

$$\mathcal{L}(\theta + \mu \Sigma^{1/2} u; \mathcal{B}) = \mathcal{L}(\theta; \mathcal{B}) + \mu \langle \mathcal{L}(\theta; \mathcal{B}), \Sigma^{1/2} u \rangle + \frac{\mu^2}{2} u^\top \Sigma^{1/2} \nabla^2 \mathcal{L}(\theta; \mathcal{B}) \Sigma^{1/2} u + \alpha(\theta, \mu \Sigma^{1/2} u). \quad (4)$$

Similarly, we also have:

$$\mathcal{L}(\theta - \mu \Sigma^{1/2} u; \mathcal{B}) = \mathcal{L}(\theta; \mathcal{B}) - \mu \langle \mathcal{L}(\theta; \mathcal{B}), \Sigma^{1/2} u \rangle + \frac{\mu^2}{2} u^\top \Sigma^{1/2} \nabla^2 \mathcal{L}(\theta; \mathcal{B}) \Sigma^{1/2} u + \alpha(\theta, -\mu \Sigma^{1/2} u).$$

Then we can calculate the difference $\Delta \mathcal{L}$ by:

$$\begin{aligned} \Delta \mathcal{L} &= \mathcal{L}(\theta + \mu \Sigma^{1/2} u; \mathcal{B}) + \mathcal{L}(\theta - \mu \Sigma^{1/2} u; \mathcal{B}) - 2\mathcal{L}(\theta; \mathcal{B}) \\ &= \mu^2 u^\top \Sigma^{1/2} \nabla^2 \mathcal{L}(\theta; \mathcal{B}) \Sigma^{1/2} u + \alpha(\theta, \mu \Sigma^{1/2} u) + \alpha(\theta, -\mu \Sigma^{1/2} u). \end{aligned}$$

Since $\alpha(\theta, \mu \Sigma^{1/2} u)$ and $\alpha(\theta, -\mu \Sigma^{1/2} u)$ are of order $\mathcal{O}(\mu^3)$, we can obtain that:

$$\frac{\Delta \mathcal{L}}{\mu^2} = u^\top \Sigma^{1/2} \nabla^2 \mathcal{L}(\theta; \mathcal{B}) \Sigma^{1/2} u + \mathcal{O}(\mu).$$

Upon substituting the above results into the left side of the Eq. (3), we arrive at:

$$\frac{1}{2} \mathbb{E} \left[\frac{\Delta \mathcal{L}}{\mu^2} \cdot \left(\Sigma^{-1/2} u u^\top \Sigma^{-1/2} - \Sigma^{-1} \right) \right] = \nabla^2 \mathcal{L}(\theta; \mathcal{B}) + \mathcal{O}(\mu).$$

Therefore, by generalizing above equation to the multi-sampling version, we can approximate the diagonal Hessian $\nabla^2 \mathcal{L}(\theta)$ at θ by:

$$\Sigma'_t(\theta) = \frac{1}{2n} \sum_{i=1}^n \left[\frac{\Delta \mathcal{L}}{\mu^2} \cdot \left(\Sigma_t^{-1/2} u_i u_i^\top \Sigma_t^{-1/2} - \Sigma^{-1} \right) \right], \quad (5)$$

where n denotes the number of sampling instances for u , indicating the frequency of estimation per step. A larger n diminishes the variance of the diagonal Hessian estimation and simultaneously increases computational overhead. Here we adopt $n = 1$ as the default setting and present the pseudo-code of HiZOO in Algorithm 1. Further experimental investigation into the impact of varying n is available in the Section 4.6.

Above equation shows that we can approximate the diagonal entries of $\nabla^2 \mathcal{L}(\theta; \mathcal{B})$ by $\text{diag}(\Sigma'_t(\theta))$, requiring just one more forward pass per step compared with MeZO.

Due to the presence of noise in the calculation of the Hessian, we utilize exponential moving average (EMA) to denoise the diagonal Hessian estimation.

$$\Sigma_{t+1}^{-1} = (1 - \alpha_t) \Sigma_t^{-1} + \alpha_t |\text{diag}(\Sigma'_t)|. \quad (6)$$

In the above equation, we firstly initial the $\Sigma_0 = I_d$ and update it every step with $\mathcal{O}(d)$ memory cost all the time. We also use $|\text{diag}(\Sigma'_t)|$ to keep all entries of Σ_t to be non-negative.

To further reduce Hessian memory consumption, we propose HiZOO-L to maintain it in a low-rank subspace, motivated by Adafactor [41]. For $\hat{\Sigma}^{-1} \in \mathbb{R}^{p \times q}$, we will store two low-rank matrices $R \in \mathbb{R}^{p \times k}$ and $C \in \mathbb{R}^{k \times q}$ with $k = 1$. Specifically, we can get $\hat{\Sigma}^{-1}$ by:

$$\hat{\Sigma}_t^{-1} = (R_t * C_t) / (1_p^\top * R_t),$$

where $1_p = (1, \dots, 1) \in \mathbb{R}^p$ denotes a column vector of p ones. Then in each step, we will update the R and C separately:

$$\begin{aligned} R_t^{-1} &= (1 - \alpha_t) R_{t-1}^{-1} + \alpha_t \left| \text{diag}(\hat{\Sigma}'_t) \right| * 1_q, \\ C_t^{-1} &= (1 - \alpha_t) C_{t-1}^{-1} + \alpha_t 1_p^\top * \left| \text{diag}(\hat{\Sigma}'_t) \right|. \end{aligned}$$

Detailed Algorithm can be seen in Appendix D.

3.4 Convergence Analysis

In this section, we will analyse the convergence based on the assumption of non-convex optimization (details in Appendix B).

Theorem 3.2. *Let the descent direction $g_\mu(\theta_t)$ defined as:*

$$g_\mu(\theta_t) = \sum_{i=1}^b \frac{\mathcal{L}(\theta_t + \mu \Sigma_t^{1/2} u_i; \mathcal{B}) - \mathcal{L}(\theta_t - \mu \Sigma_t^{1/2} u_i; \mathcal{B})}{2b\mu} \Sigma_t^{1/2} u_i. \quad (7)$$

Based on Assumption B.1-B.3, if the update rule for θ is $\theta_{t+1} = \theta_t - \eta g_\mu(\theta_t)$ for a single step, then it's established that:

$$\mathbb{E} [\mathcal{L}(\theta_{t+1}; \mathcal{B})] \leq \mathcal{L}(\theta_t; \mathcal{B}) - \frac{\eta_t}{4} \|\nabla \mathcal{L}(\theta_t; \mathcal{B})\|_{\Sigma_t}^2 + 2\eta_t^2 L (\text{tr}(\Sigma_t) + \beta_u) \sigma^2 + \mathcal{O}(\mu^2). \quad (8)$$

Furthermore, given iteration number T , we choose the step size $\eta = \frac{1}{8\sqrt{T}L(\max_t \text{tr}(\Sigma_t) + \beta_u)}$ and take $\theta_{out} = \theta_j$ with j uniformly sampled from $\{1, \dots, T\}$. Then, we have

$$\mathbb{E} [\|\nabla \mathcal{L}(\theta_{out}; \mathcal{B})\|^2] \leq \frac{32L(\max_t \{\text{tr}(\Sigma_t)\} + \beta_u)(\mathcal{L}(\theta_1; \mathcal{B}) - \mathcal{L}(\theta_*; \mathcal{B}))}{\sqrt{T}\beta_\ell} + \frac{\sigma^2}{T^{3/2}\beta_\ell} + \mathcal{O}(\mu^2), \quad (9)$$

where $\mathcal{L}(\theta_; \mathcal{B})$ minimizes the function $\mathcal{L}(\theta; \mathcal{B})$. The above equation shows that as $T \rightarrow \infty$, HiZOO can converge to the optimum point.*

Proof. Detailed proof can be found in Appendix B. □

3.5 Visualization of HiZOO on Test Functions

Despite above theoretical guarantee, **we still want to illustrate how HiZOO utilizes Hessian to improve the convergence process**. But it's impractical for large models to visualize their optimization trajectories. Therefore we choose three test functions (see details in Appendix C) with heterogeneous curvatures across different parameters and visualize the optimization trajectories on them.

As illustrated in Figure 3, HiZOO and Adam both achieve better convergence on three functions, and HiZOO even requires less steps for convergence than Adam. However, MeZO only achieves effective convergence in either the x or y dimension, but not both, indicating a limitation in capturing this curvature difference. Particularly in function (c) curvature of x is extremely bigger than y . In this case, HiZOO can sense this difference in parametric curvature and update the function along x on purpose, achieving quicker convergence. In contrast, MeZO is very hard to converge.

4 Experiments

Large language models are generally classified into two types: (1) Encoder-Decoder, also known as masked language models, such as BERT [11] and ALBERT [23]; (2) Decoder-Only, also recognized as generative language models, such as GPT family [37, 3], OPT [57], LLaMA [45], Phi [25, 17].

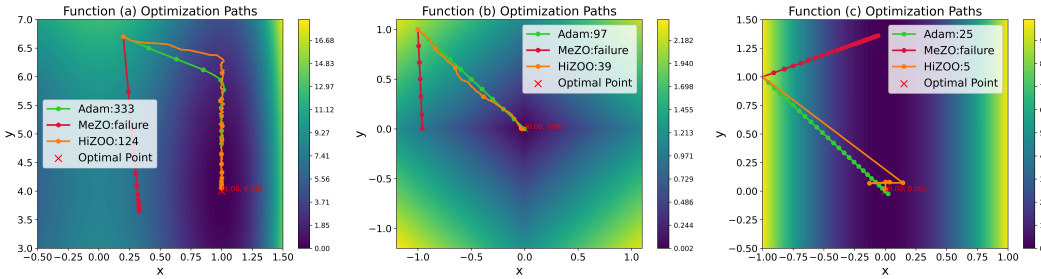


Figure 3: Optimization trajectories of Adam, MeZO and HiZOO on 3 test functions. We have labeled the number of iterations required for the loss to drop to 0.1.

To rigorously assess the universality and robustness of our HiZOO, we have chosen models from each category for empirical testing. Additionally, we investigate FT and PEFT (LoRA [19] and prefix [24]). Detailed experiment settings are presented in Appendix E.1.

4.1 Masked Language Models

Firstly, we conduct experiments on RoBERTa-large 350M [28] on three NLP task paradigms: sentence classification, multiple choice and text generation. We follow the experimental setting [32] in studying the few-shot and many-shot, sampling k examples per class for $k = 16$ (results in Table 1), which can reach the following observations and summaries.

Task Type	SST-2	SST-5	SNLI	MNLI	RTE	TREC	Average
	— sentiment —		— natural language inference —			— topic —	
Zero-shot	79.0	35.5	50.2	48.8	51.4	32.0	49.5
LP	76.0 (± 2.8)	40.3 (± 1.9)	66.0 (± 2.7)	56.5 (± 2.5)	59.4 (± 5.3)	51.3 (± 5.5)	58.3
FT	91.9 (± 1.8)	47.5 (± 1.9)	77.5 (± 2.6)	70.0 (± 2.3)	66.4 (± 7.2)	85.0 (± 2.5)	74.9
PEFT	91.9 (± 1.0)	47.7 (± 1.1)	77.2 (± 1.3)	67.7 (± 1.4)	66.6 (± 2.0)	85.7 (± 1.3)	72.8
MeZO	90.5 (± 1.2)	45.5 (± 2.0)	68.5 (± 3.9)	58.7 (± 2.5)	64.0 (± 3.3)	76.9 (± 2.7)	67.4
MeZO (PEFT)	91.4 (± 0.9)	45.8 (± 2.0)	71.6 (± 2.5)	64.0 (± 2.5)	65.4 (± 3.9)	80.3 (± 3.6)	69.8
HiZOO	93.2 (± 0.8)	46.2 (± 1.1)	74.6 (± 1.3)	64.9 (± 1.7)	66.8 (± 1.2)	79.8 (± 1.3)	70.9
HiZOO(PEFT)	92.3 (± 1.2)	47.2 (± 1.1)	71.1 (± 1.1)	62.1 (± 1.7)	65.4 (± 1.2)	82.0 (± 2.0)	70.0

Table 1: Experiments on RoBERTa-large (350M parameters, $k=16$). PEFT represents the LoRA and prefix and we report the best of them. All reported numbers are averaged accuracy (standard deviation) across 5 runs.

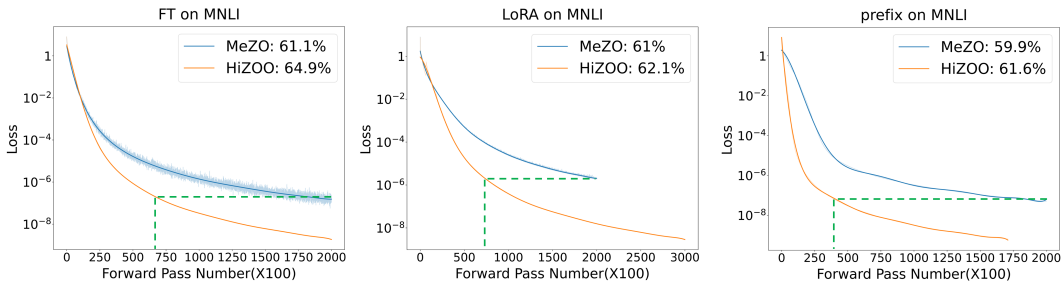


Figure 4: OPT-13B results with zero-shot, in-context learning (ICL), MeZO, HiZOO and fine-tuning with Adam (FT). PEFT represents the best among LoRA and prefix. More details can be found in Appendix E.2.

HiZOO greatly increases the convergence speed across full-parameter tuning, LoRA and prefix. As shown in Figure 4, HiZOO achieves 4 \times speedup over MeZO on average while getting the same training loss compared with MeZO. What's more, HiZOO finally achieves a 1.57% accuracy improvement better than MeZO. More loss curves can be seen in Appendix E.1.

HiZOO achieves better performance compared with MeZO. Table 1 shows that HiZOO outperforms MeZO’s results with 3.5% on average on all datasets across different tasks. Specifically, HiZOO outperforms MeZO more than 6% in accuon SNLI and MNLI dataset.

4.2 Auto-Regressive Language Models

Then we extend experiments with OPT family (13B, 30B, 66B) on the same NLP task paradigms. The main results on OPT-13B are presented in Table 2. We can see that HiZOO boosts MeZO’s accuracy for 1.1% accuracy on average using prefix-tuning. Specifically, HiZOO achieves 2.87% and 3% accuracy improvement on WSC and COPA tasks.

HiZOO is capable of scaling to large models with up to 66B parameters, while preserving its exceptional performance. As depicted in Table 3, on OPT-30B HiZOO outperforms MeZO with up to 2.9% increase and 0.8% increase on average. Even scaling to OPT-66B, HiZOO(prefix) still outperforms MeZO(prefix) with up to 5.1% increase and 2% increase on average.

In addition, We utilize HiZOO to fine-tune the newly proposed model, Phi-2 (2.7B) and Llama3 (8B). Experiment results in Table 2 show that HiZOO outperforms MeZO in most cases. We also provide relative loss curves to show the better convergence process of our HiZOO in Appendix E.3.

Table 2: Experiments on three different models(with 1000 examples). We highlight the best results between MeZO, HiZOO and HiZOO-L in bold to facilitate comparison.

Model	Method	SST-2	RTE	CB	WSC	WIC	COPA	MultiRC	Average
Phi-2	MeZO	86.6	67.1	75.0	59.6	54.4	86.0	78.2	72.4
Phi-2	HiZOO	88.9	69.0	75.2	62.5	59.4	86.0	79.2	74.3
Phi-2	HiZOO-L	88.9	68.9	75.2	62.4	59.2	86.0	79.2	74.2
Llama3	MeZO	92.2	74.4	69.6	63.5	57.8	88.0	77.6	74.7
Llama3	HiZOO	93.5	75.1	69.6	63.5	59.7	89.0	78.2	75.5
Llama3	HiZOO-L	94.3	75.1	69.6	63.5	57.7	89.0	77.9	75.3
OPT-13B	MeZO	91.4	66.1	66.0	63.5	59.4	88.0	57.3	70.2
OPT-13B	HiZOO	92.1	69.3	69.6	63.5	59.4	89.0	61.3	72.1
OPT-13B	HiZOO-L	92.1	68.2	67.9	65.4	59.4	89.0	61.1	71.9

4.3 Training with Non-Differentiable Objectives

Our proposed HiZOO employs gradient estimation to update parameters, allowing for the use of non-differentiable objectives for training. Following the setting of MeZO [32], we conduct extensive experiments using F1 as optimization objective. The results presented in Table 4 indicate that our method outperforms MeZO by **6.36%** on F1 on average.

Table 3: Experiments on OPT-30B (we use FT and prefix-tuning, report the best of them) and OPT-66B (we use prefix-tuning).

Task	SST-2	RTE	WSC	WIC	Average
30B MeZO	90.6	66.4	63.5	59.1	69.9
30B HiZOO	91.2	69.3	63.5	60.2	71.0
30B HiZOO-L	91.1	68.9	63.5	59.8	70.8
66B MeZO	93.6	66.4	57.7	58.6	69.0
66B HiZOO	93.6	71.5	60.6	61.1	71.7
66B HiZOO-L	93.6	71.0	60.3	60.9	71.4

Table 4: Experiments on non-differentiable optimization objectives (F1). For classification ($k = 512$), we use full-parameter tuning and for SQuAD (1,000 examples), we use prefix tuning.

Model	RoBERTa-large (350M)				OPT-13B
	SST-2	SST-5	SNLI	TREC	
Zero-shot	79.0	35.5	50.2	32.0	46.2
MeZO	92.7	48.9	82.7	68.6	78.5
HiZOO	94.9	52.9	83.1	90	83.21

4.4 Memory Usage and Time Efficiency Analysis

Memory Usage As shown in Figure 5, HiZOO increases the memory usage compared to MeZO because of the storage of the diagonal Hessian(refer to Appendix F for detailed numbers). To further reduce memory consumption, we propose HiZOO-L, the low-rank implementation of HiZOO, motivated by Adafactor [41]. Detailed Algorithm can be seen in Appendix D. As a result, HiZOO-L increases < 10% memory more than MeZO, while maintaining the original performance of HiZOO, as shown in Figure 5. Specifically, using the same GPUs, HiZOO-L allows for tuning a model that is 10 times larger than what is feasible with FT on average.

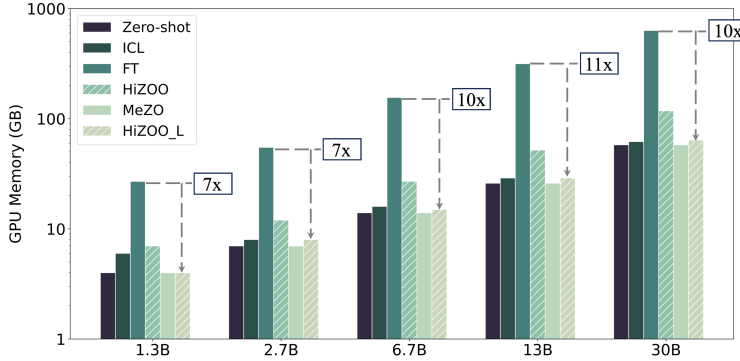


Figure 5: GPU memory consumption with different OPT models and tuning methods on MultiRC (400 tokens per example on average). More details can be found in Appendix F.

Time Efficiency In Appendix F, we analyse the wall-clock time efficiencies and show that HiZOO spends $1.5\times$ time per step compared with MeZO, mainly from the extra forward pass. However, HiZOO reduces total number of forward passes required for convergence. For example, HiZOO achieves a $8\times$ and $4\times$ speedup on SST2 and MNLI tasks.

4.5 Comparison with other ZO variants

We also compare our HiZOO with a broader array of ZO optimization techniques [59]. As shown in Table 5, our HiZOO outperforms all other ZO methods. Compared with ZO-Adam who leverages second-order moment to guide gradient descent, our HiZOO-L achieves a notable **4.3%** absolute improvement, while using **50%** of the GPU memory.

Table 5: Performance comparison on SST2(Robert-Large and OPT-1.3B) and COPA(OPT-13B) using different ZO methods. Memory and runtime cost are multiples of ZO-SGD.

Model/Task	Roberts-Large		OPT-1.3B		OPT-13B		Average	Memory	Runtime
	FT	prefix	FT	prefix	FT	prefix			
ZO-SGD	89.4	90.0	90.8	91.4	90.0	79.0	88.4	1.0x	1.0x
ZO-SGD-MMT	89.6	89.1	85.2	91.2	87.0	85.0	87.8	1.56x	1.0x
ZO-SGD-Cons	89.6	89.1	88.3	88.1	82.0	84.0	86.8	1.0x	2.49x
ZO-SGD-Sign	52.5	53.6	87.2	89.5	80.0	78.0	73.4	1.0x	1.0x
ZO-Adam	89.8	90.2	84.4	91.4	82.0	79.0	86.1	2.47x	1.04x
HiZOO	93.2	92.7	90.7	91.4	88.0	87.0	90.5	2.04x	1.37x
HiZOO-L	92.5	92.7	90.7	91.4	88.0	87.0	90.4	1.12x	1.39x

4.6 Hyperparameter Analysis

Influence of Smooth Scale α_t in EMA To assess the robustness of the optimizer, a grid search is conducted to evaluate the sensitivity of the hyper-parameter α_t on RoBERTa-large (350M). Figure 6 illustrates that the smoothing scale α_t is instrumental in controlling the convergence rate during training. As α_t is incrementally increased from zero, the training loss decreases faster. However, too large α_t values may impede convergence or even cause training to fail due to gradient explosion.

Influence of Estimation Times n Per Step We also propose a variant of HiZOO in Appendix D.1: HiZOO-multi, which has $n > 1$ per step. As shown in Figure 7, different n maybe doesn't affect the final accuracy. However, the larger n will estimate the diagonal Hessian more accurate per step and accelerate model convergence, reducing the overall training steps. But it will also increase the computation per step. Balancing these factors is crucial for efficient training.

5 Conclusion

In this work, we introduce HiZOO, which is the first ZOO that incorporates diagonal Hessian for fine-tuning LLMs. By introducing one more forward pass, HiZOO can handle heterogeneous curvatures across different parameter dimensions. We provide theoretical analysis and visualize

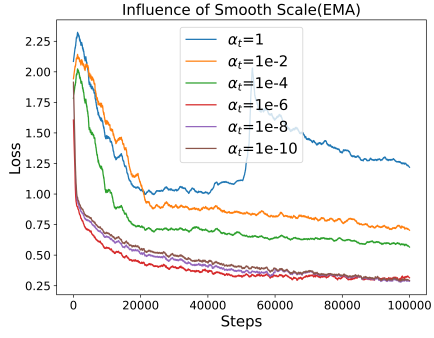


Figure 6: Experiments on influence of EMA α_t for hessian in Eq. (6). We use HiZOO (prefix) to fine-tune Roberta-large on SNLI. More results can be found in Appendix H.1.

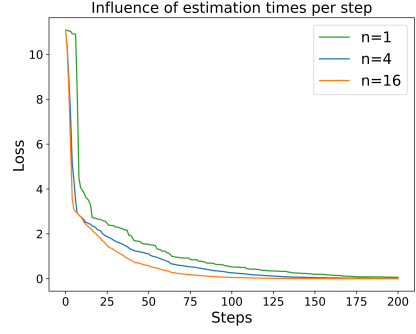


Figure 7: Loss curves on Function (a) using the variant HiZOO-multi with different estimation times n per step. Trajectory visualization can be found in Appendix D.1.

the optimization trajectories to explore how it works. Further experiments on LLMs show that HiZOO converges in much fewer steps than MeZO and achieves better performance, across various models (RoBERTa-large, OPT, Llama3, Phi-2) and methods (FT, LoRA and prefix). In addition, HiZOO increases extra memory cost because of the storage of Hessian. We explore a memory efficient implementation (HiZOO-L) and there are many other methods worth trying, such as quantization [10], FlashAttention [8].

References

- [1] A. Agarwal, M. J. Wainwright, P. Bartlett, and P. Ravikumar. Information-theoretic lower bounds on the oracle complexity of convex optimization. *Advances in Neural Information Processing Systems*, 22, 2009.
- [2] R. Anil, V. Gupta, T. Koren, K. Regan, and Y. Singer. Scalable second order optimization for deep learning, 2021.
- [3] T. B. Brown, B. Mann, N. Ryder, M. Subbiah, J. Kaplan, P. Dhariwal, A. Neelakantan, P. Shyam, G. Sastry, A. Askell, S. Agarwal, A. Herbert-Voss, G. Krueger, T. Henighan, R. Child, A. Ramesh, D. M. Ziegler, J. Wu, C. Winter, C. Hesse, M. Chen, E. Sigler, M. Litwin, S. Gray, B. Chess, J. Clark, C. Berner, S. McCandlish, A. Radford, I. Sutskever, and D. Amodei. Language models are few-shot learners, 2020.
- [4] C. G. BROYDEN. The Convergence of a Class of Double-rank Minimization Algorithms 1. General Considerations. *IMA Journal of Applied Mathematics*, 6(1):76–90, 03 1970. ISSN 0272-4960. doi: 10.1093/imamat/6.1.76. URL <https://doi.org/10.1093/imamat/6.1.76>.
- [5] H. Cai, Y. Lou, D. Mckenzie, and W. Yin. A zeroth-order block coordinate descent algorithm for huge-scale black-box optimization. In M. Meila and T. Zhang, editors, *Proceedings of the 38th International Conference on Machine Learning*, volume 139 of *Proceedings of Machine Learning Research*, pages 1193–1203. PMLR, 18–24 Jul 2021.
- [6] P.-Y. Chen, H. Zhang, Y. Sharma, J. Yi, and C.-J. Hsieh. Zoo: Zeroth order optimization based black-box attacks to deep neural networks without training substitute models. New York, NY, USA, 2017. Association for Computing Machinery. ISBN 9781450352024. doi: 10.1145/3128572.3140448. URL <https://doi.org/10.1145/3128572.3140448>.
- [7] A. R. Conn, N. I. M. Gould, and P. L. Toint. *Trust-Region Methods*. Society for Industrial and Applied Mathematics, USA, 2000. ISBN 0898714605.
- [8] T. Dao, D. Y. Fu, S. Ermon, A. Rudra, and C. Ré. Flashattention: Fast and memory-efficient exact attention with io-awareness, 2022.
- [9] R. S. Dembo, S. C. Eisenstat, and T. Steihaug. Inexact newton methods. *SIAM Journal on Numerical Analysis*, 19(2):400–408, 1982. doi: 10.1137/0719025. URL <https://doi.org/10.1137/0719025>.
- [10] T. Dettmers, A. Pagnoni, A. Holtzman, and L. Zettlemoyer. Qlora: Efficient finetuning of quantized llms, 2023.
- [11] J. Devlin, M.-W. Chang, K. Lee, and K. Toutanova. Bert: Pre-training of deep bidirectional transformers for language understanding. In *North American Chapter of the Association for Computational Linguistics*, 2019. URL <https://api.semanticscholar.org/CorpusID:52967399>.
- [12] J. Duchi, E. Hazan, and Y. Singer. Adaptive subgradient methods for online learning and stochastic optimization. *J. Mach. Learn. Res.*, 12(null):2121–2159, jul 2011. ISSN 1532-4435.
- [13] FairScale authors. Fairscale: A general purpose modular pytorch library for high performance and large scale training. <https://github.com/facebookresearch/fairscale>, 2021.
- [14] T. George, C. Laurent, X. Bouthillier, N. Ballas, and P. Vincent. Fast approximate natural gradient descent in a kronecker-factored eigenbasis. In *Proceedings of the 32nd International Conference on Neural Information Processing Systems*, NIPS’18, page 9573–9583, Red Hook, NY, USA, 2018. Curran Associates Inc.
- [15] S. Ghadimi and G. Lan. Stochastic first-and zeroth-order methods for nonconvex stochastic programming. *SIAM Journal on Optimization*, 23(4):2341–2368, 2013.

[16] B. Ghorbani, S. Krishnan, and Y. Xiao. An investigation into neural net optimization via hessian eigenvalue density. In K. Chaudhuri and R. Salakhutdinov, editors, *Proceedings of the 36th International Conference on Machine Learning*, volume 97 of *Proceedings of Machine Learning Research*, pages 2232–2241. PMLR, 09–15 Jun 2019. URL <https://proceedings.mlr.press/v97/ghorbani19b.html>.

[17] S. Gunasekar, Y. Zhang, J. Aneja, C. C. T. Mendes, A. D. Giorno, S. Gopi, M. Javaheripi, P. Kauffmann, G. de Rosa, O. Saarikivi, A. Salim, S. Shah, H. S. Behl, X. Wang, S. Bubeck, R. Eldan, A. T. Kalai, Y. T. Lee, and Y. Li. Textbooks are all you need, 2023.

[18] D. Hajinezhad and M. M. Zavlanos. Gradient-free multi-agent nonconvex nonsmooth optimization. *2018 IEEE Conference on Decision and Control (CDC)*, pages 4939–4944, 2018. URL <https://api.semanticscholar.org/CorpusID:58669445>.

[19] E. J. Hu, yelong shen, P. Wallis, Z. Allen-Zhu, Y. Li, S. Wang, L. Wang, and W. Chen. LoRA: Low-rank adaptation of large language models. In *International Conference on Learning Representations*, 2022. URL <https://openreview.net/forum?id=nZeVKeeFYf9>.

[20] K. G. Jamieson, R. Nowak, and B. Recht. Query complexity of derivative-free optimization. *Advances in Neural Information Processing Systems*, 25, 2012.

[21] S. Jiang, Q. Chen, Y. Pan, Y. Xiang, Y. Lin, X. Wu, C. Liu, and X. Song. Zo-adam: Zo-adam optimizer: Adapting perturbation by the momentum and uncertainty in zeroth-order optimization, 2023.

[22] D. Kingma and J. Ba. Adam: A method for stochastic optimization. In *International Conference on Learning Representations (ICLR)*, San Diego, CA, USA, 2015.

[23] Z. Lan, M. Chen, S. Goodman, K. Gimpel, P. Sharma, and R. Soricut. Albert: A lite bert for self-supervised learning of language representations. In *International Conference on Learning Representations*, 2020. URL <https://openreview.net/forum?id=H1eA7AEtvS>.

[24] X. L. Li and P. Liang. Prefix-tuning: Optimizing continuous prompts for generation. In C. Zong, F. Xia, W. Li, and R. Navigli, editors, *Proceedings of the 59th Annual Meeting of the Association for Computational Linguistics and the 11th International Joint Conference on Natural Language Processing (Volume 1: Long Papers)*, pages 4582–4597, Online, Aug. 2021. Association for Computational Linguistics. doi: 10.18653/v1/2021.acl-long.353. URL <https://aclanthology.org/2021.acl-long.353>.

[25] Y. Li, S. Bubeck, R. Eldan, A. D. Giorno, S. Gunasekar, and Y. T. Lee. Textbooks are all you need ii: phi-1.5 technical report, 2023.

[26] H. Liu and Z. Li. Sophia: A scalable stochastic second-order optimizer for language model pre-training. <https://synthical.com/article/17aca766-2012-4c7c-a0f4-5b785dadabf9>, 4 2023.

[27] S. Liu, P.-Y. Chen, X. Chen, and M. Hong. signs gd via zeroth-order oracle. In *International Conference on Learning Representations*, 2019. URL <https://api.semanticscholar.org/CorpusID:108298677>.

[28] Y. Liu, M. Ott, N. Goyal, J. Du, M. Joshi, D. Chen, O. Levy, M. Lewis, L. Zettlemoyer, and V. Stoyanov. Roberta: A robustly optimized bert pretraining approach. *arXiv preprint arXiv:1907.11692*, 2019.

[29] I. Loshchilov and F. Hutter. Decoupled weight decay regularization. In *International Conference on Learning Representations*, 2019. URL <https://openreview.net/forum?id=Bkg6RiCqY7>.

[30] J. R. Magnus et al. *The moments of products of quadratic forms in normal variables*. Univ., Instituut voor Actuariaat en Econometrie, 1978.

[31] G. D. Magoulas, M. N. Vrahatis, and G. S. Androutsakis. Improving the convergence of the backpropagation algorithm using learning rate adaptation methods. *Neural Comput.*, 11(7):1769–1796, oct 1999. ISSN 0899-7667. doi: 10.1162/089976699300016223. URL <https://doi.org/10.1162/089976699300016223>.

[32] S. Malladi, T. Gao, E. Nichani, A. Damian, J. D. Lee, D. Chen, and S. Arora. Fine-tuning language models with just forward passes. In *Thirty-seventh Conference on Neural Information Processing Systems*, 2023. URL <https://openreview.net/forum?id=Vota6rFhBQ>.

[33] J. Martens. Deep learning via hessian-free optimization. In *Proceedings of the 27th International Conference on International Conference on Machine Learning*, ICML’10, page 735–742, Madison, WI, USA, 2010. Omnipress. ISBN 9781605589077.

[34] Y. Nesterov and B. T. Polyak. Cubic regularization of newton method and its global performance. *Math. Program.*, 108(1):177–205, aug 2006. ISSN 0025-5610.

[35] R. Pan, X. Liu, S. Diao, R. Pi, J. Zhang, C. Han, and T. Zhang. Lisa: Layerwise importance sampling for memory-efficient large language model fine-tuning, 2024.

[36] R. Pascanu and Y. Bengio. Revisiting natural gradient for deep networks, 2014.

[37] A. Radford, J. Wu, R. Child, D. Luan, D. Amodei, and I. Sutskever. Language models are unsupervised multitask learners. 2019.

[38] M. Raginsky and A. Rakhlin. Information-based complexity, feedback and dynamics in convex programming. *IEEE Transactions on Information Theory*, 57(10):7036–7056, 2011.

[39] L. Sagun, L. Bottou, and Y. LeCun. Eigenvalues of the hessian in deep learning: Singularity and beyond, 2017. URL <https://openreview.net/forum?id=B186cP9gx>.

[40] T. Schaul, S. Zhang, and Y. LeCun. No more pesky learning rates. In S. Dasgupta and D. McAllester, editors, *Proceedings of the 30th International Conference on Machine Learning*, volume 28 of *Proceedings of Machine Learning Research*, pages 343–351, Atlanta, Georgia, USA, 17–19 Jun 2013. PMLR. URL <https://proceedings.mlr.press/v28/schaul13.html>.

[41] N. Shazeer and M. Stern. Adafactor: Adaptive learning rates with sublinear memory cost. In J. Dy and A. Krause, editors, *Proceedings of the 35th International Conference on Machine Learning*, volume 80 of *Proceedings of Machine Learning Research*, pages 4596–4604. PMLR, 10–15 Jul 2018. URL <https://proceedings.mlr.press/v80/shazeer18a.html>.

[42] J. Spall. Multivariate stochastic approximation using a simultaneous perturbation gradient approximation. *IEEE Transactions on Automatic Control*, 37(3):332–341, 1992. doi: 10.1109/9.119632.

[43] J. C. Spall. A one-measurement form of simultaneous perturbation stochastic approximation. *Automatica*, 33(1):109–112, jan 1997. ISSN 0005-1098. doi: 10.1016/S0005-1098(96)00149-5. URL [https://doi.org/10.1016/S0005-1098\(96\)00149-5](https://doi.org/10.1016/S0005-1098(96)00149-5).

[44] Y. Tang, J. Zhang, and N. Li. Distributed zero-order algorithms for nonconvex multiagent optimization. *IEEE Transactions on Control of Network Systems*, 8(1):269–281, 2021. doi: 10.1109/TCNS.2020.3024321.

[45] H. Touvron, T. Lavril, G. Izacard, X. Martinet, M.-A. Lachaux, T. Lacroix, B. Rozière, N. Goyal, E. Hambro, F. Azhar, A. Rodriguez, A. Joulin, E. Grave, and G. Lample. Llama: Open and efficient foundation language models. *ArXiv*, abs/2302.13971, 2023. URL <https://api.semanticscholar.org/CorpusID:257219404>.

[46] A. T. Vakhitov, O. N. Granichin, and L. S. Gurevich. Algorithm for stochastic approximation with trial input perturbation in the nonstationary problem of optimization. *Autom. Remote Control*, 70(11):1827–1835, nov 2009. ISSN 0005-1179. doi: 10.1134/S000511790911006X. URL <https://doi.org/10.1134/S000511790911006X>.

[47] Z. Wang, K. Balasubramanian, S. Ma, and M. Razaviyayn. Zeroth-order algorithms for nonconvex minimax problems with improved complexities. *arXiv preprint arXiv:2001.07819*, 2020.

[48] P. Xu, F. Roosta, and M. W. Mahoney. Newton-type methods for non-convex optimization under inexact hessian information, 2019.

[49] Z. Yao, P. Xu, F. Roosta-Khorasani, and M. W. Mahoney. Inexact non-convex newton-type methods, 2018.

[50] Z. Yao, A. Gholami, S. Shen, M. Mustafa, K. Keutzer, and M. Mahoney. Adahessian: An adaptive second order optimizer for machine learning. *Proceedings of the AAAI Conference on Artificial Intelligence*, 35(12):10665–10673, May 2021. doi: 10.1609/aaai.v35i12.17275. URL <https://ojs.aaai.org/index.php/AAAI/article/view/17275>.

[51] H. Ye. Mirror natural evolution strategies, 2023.

[52] H. Ye, Z. Huang, C. Fang, C. J. Li, and T. Zhang. Hessian-aware zeroth-order optimization for black-box adversarial attack, 2019.

[53] Y. You, J. Li, S. Reddi, J. Hseu, S. Kumar, S. Bhojanapalli, X. Song, J. Demmel, K. Keutzer, and C.-J. Hsieh. Large batch optimization for deep learning: Training bert in 76 minutes. In *International Conference on Learning Representations*, 2020. URL <https://openreview.net/forum?id=Syx4wnEtvH>.

[54] M. D. Zeiler. Adadelta: An adaptive learning rate method, 2012.

[55] J. Zhang, S. P. Karimireddy, A. Veit, S. Kim, S. Reddi, S. Kumar, and S. Sra. Why are adaptive methods good for attention models? In H. Larochelle, M. Ranzato, R. Hadsell, M. Balcan, and H. Lin, editors, *Advances in Neural Information Processing Systems*, volume 33, pages 15383–15393. Curran Associates, Inc., 2020. URL https://proceedings.neurips.cc/paper_files/paper/2020/file/b05b57f6add810d3b7490866d74c0053-Paper.pdf.

[56] L. Zhang, S. Shi, and B. Li. Eva: Practical second-order optimization with kronecker-vectorized approximation. In *The Eleventh International Conference on Learning Representations*, 2023. URL https://openreview.net/forum?id=_Mic8V96Voy.

[57] S. Zhang, S. Roller, N. Goyal, M. Artetxe, M. Chen, S. Chen, C. Dewan, M. Diab, X. Li, X. V. Lin, T. Mihaylov, M. Ott, S. Shleifer, K. Shuster, D. Simig, P. S. Koura, A. Sridhar, T. Wang, and L. Zettlemoyer. Opt: Open pre-trained transformer language models, 2022.

[58] Y. Zhang, Y. Zhou, K. Ji, and M. M. Zavlanos. A new one-point residual-feedback oracle for black-box learning and control. *Automatica*, 136(C), feb 2022. ISSN 0005-1098. doi: 10.1016/j.automatica.2021.110006. URL <https://doi.org/10.1016/j.automatica.2021.110006>.

[59] Y. Zhang, P. Li, J. Hong, J. Li, Y. Zhang, W. Zheng, P.-Y. Chen, J. D. Lee, W. Yin, M. Hong, Z. Wang, S. Liu, and T. Chen. Revisiting zeroth-order optimization for memory-efficient llm fine-tuning: A benchmark, 2024. URL <https://arxiv.org/abs/2402.11592>.

[60] J. Zhao, Z. Zhang, B. Chen, Z. Wang, A. Anandkumar, and Y. Tian. Galore: Memory-efficient llm training by gradient low-rank projection, 2024.

A Related Works

A.1 First-order Optimizer Used in LLMs

Optimization methods have consistently been a popular research domain, encompassing techniques such as Gradient Descent (GD), Momentum, Adagrad [12], ADADELTA [54], and Newton’s method, which have been instrumental in advancing fields like computer vision. However, the emergence of large-scale models, characterized by their massive parameter counts and intricate architectures, has challenged the efficacy of conventional optimization methods for training tasks. Amidst this landscape, Adam [22] has emerged as the preferred choice for its ability to rapidly converge, making it particularly suitable for the training and fine-tuning large models. Then AdamW [29] was proposed to add a weight decay coefficient to alleviate over-fitting. Notwithstanding these advancements, a limitation persists with these optimizers: they have an implicit batch size ceiling. Exceeding this threshold can provoke extreme gradient updates, thus impeding the convergence rate of the models. This bottleneck is particularly problematic in the context of large-model training, which typically necessitates substantial batch sizes. To circumvent this constraint, LAMB [53] was devised to apply principled layer-wise adaptation strategy to accelerate the training of large models employing large batches.

A.2 Hessian Based First-Order Optimizer

Compared with first-order optimizers, second-order optimizer considers second-order information in the process of gradient calculation. As a result, it has more abundant information to guide gradient descent and is considered to be more promising. Previous studies utilized curvature information to pre-condition the gradient [4, 34, 7]. Subsequently, Magoulas et al. [31] applied diagonal Hessian as the pre-conditioner, which greatly promotes the landing of second-order optimizer in the field of deep learning. Martens [33] approximated the Hessian with conjugate gradient. Schaul et al. [40] utilized diagonal Hessian to automatically adjust the learning rate of SGD during training. Another work [36] extended natural gradient descent to incorporate second order information alongside the manifold information and used a truncated Newton approach for inverting the metric matrix instead of using a diagonal approximation of it. EVA [56] proposed to use the Kronecker factorization of two small vectors to approximate the Hessian, which significantly reduces memory consumption. AdaHessian [50] incorporates an approximate Hessian diagonal, with spatial averaging and momentum to precondition the gradient vector.

Although great progress has been made in the research of second-order optimizer, it has not been widely used because of the extra computation and memory cost when gradient updating, and this situation is extremely serious in the training of large language models. Based on the above dilemma, recent works [2, 14] proposed to offload Hessian computation to CPUs and utilized ResNets and very large batch size to approximate the Fisher information matrix. Sophia [26] was the first to apply second-order optimizer and achieve a speed-up on large language models in total compute successfully.

A.3 Zeroth-Order Optimizer

Zeroth-order optimization, is also known as derivative-free or black-box optimization. There have been many one-point gradient estimators in past works [13, 43, 46, 42, 20, 1, 38, 47]. However, cursory experiments with one such promising estimator [58] reveal that SPSA outperforms other methods.

In previous works, it appears in a wide range of applications where either the objective function is implicit or its gradient is impossible or too expensive to compute. For example, methods [44, 18] consider derivative-free distributed algorithms for non-convex multi-agent optimization. ZO-BCD[5], ZOO[6], ZO-signSGD [27] and ZO-HessAware [52] utilize zeroth-order stochastic optimization to generate black-box adversarial example in deep learning.

Beyond that, MeZO [32] firstly adapted the classical ZO-SGD method to fine-tune LLMs, while achieving comparable performance with extremely great memory reduction and GPU-hour reduction. Subsequently, ZO-AdaMU [21] improved ZO-SGD and adapted the simulated perturbation with momentum in its stochastic approximation method. Both of these two optimizers provide researchers with a new and promising technique for fine-tuning large models.

B Detailed Convergence Analysis

Firstly, our convergence analysis requires the following assumptions:

Assumption B.1. The objective function $\mathcal{L}(\theta; \mathcal{B})$ is L -smooth, which means that for any $\theta_1, \theta_2 \in \mathbb{R}^d$, it holds that:

$$\mathcal{L}(\theta_2; \mathcal{B}) \leq \mathcal{L}(\theta_1; \mathcal{B}) + \langle \nabla \mathcal{L}(\theta_1; \mathcal{B}), \theta_2 - \theta_1 \rangle + \frac{L}{2} \|\theta_2 - \theta_1\|^2. \quad (10)$$

Assumption B.2. The stochastic gradient $\nabla \mathcal{L}(\theta; \mathcal{B})$ has σ^2 variance, which means:

$$\mathbb{E} [\|\nabla \mathcal{L}(\theta; \mathcal{B}) - \nabla \mathcal{L}(\theta)\|^2] \leq \sigma^2. \quad (11)$$

Assumption B.3. Each entry of Σ_t lies in the range $[\beta_\ell, \beta_u]$ with $0 < \beta_\ell \leq \beta_u$.

Then we will give the detailed proof for convergence.

Proof. By the update rule of θ_t and Assumption B.1, we have

$$\begin{aligned} & \mathbb{E} [\mathcal{L}(\theta_{t+1}; \mathcal{B}_{t+1}) \mid \theta_t] \\ & \leq \mathcal{L}(\theta_t; \mathcal{B}_t) - \eta_t \mathbb{E} [\langle \nabla \mathcal{L}(\theta_t; \mathcal{B}_t), g_\mu(\theta_t) \rangle] + \frac{L\eta_t^2}{2} \mathbb{E} [\|g_\mu(\theta_t)\|^2] \\ & \leq \mathcal{L}(\theta_t; \mathcal{B}_t) - \eta_t \|\nabla \mathcal{L}(\theta_t; \mathcal{B}_t)\|_{\Sigma_t}^2 + \eta_t \mathcal{O}(\mu \|\nabla \mathcal{L}(\theta_t; \mathcal{B}_t)\|) \\ & \quad + 2\eta_t^2 L (\text{tr}(\Sigma_t) + \beta_u) \|\nabla \mathcal{L}(\theta_t; \mathcal{B}_t)\|_{\Sigma_t}^2 \\ & \quad + 2\eta_t^2 L (\text{tr}(\Sigma_t) + \beta_u) \sigma^2 + \mathcal{O}(\mu^2) \\ & \leq \mathcal{L}(\theta_t; \mathcal{B}_t) - \frac{\eta_t}{2} \|\nabla \mathcal{L}(\theta_t; \mathcal{B}_t)\|_{\Sigma_t}^2 + 2\eta_t^2 L (\text{tr}(\Sigma_t) + \beta_u) \|\nabla \mathcal{L}(\theta_t; \mathcal{B}_t)\|_{\Sigma_t}^2 \\ & \quad + 2\eta_t^2 L (\text{tr}(\Sigma_t) + \beta_u) \sigma^2 + \mathcal{O}(\mu^2) \\ & = \mathcal{L}(\theta_t; \mathcal{B}_t) - \frac{\eta_t}{2} (1 - 4\eta_t L (\text{tr}(\Sigma_t) + \beta_u)) \|\nabla \mathcal{L}(\theta_t; \mathcal{B}_t)\|_{\Sigma_t}^2 \\ & \quad + 2\eta_t^2 L (\text{tr}(\Sigma_t) + \beta_u) \sigma^2 + \mathcal{O}(\mu^2) \\ & \leq \mathcal{L}(\theta_t; \mathcal{B}_t) - \frac{\eta_t}{4} \|\nabla \mathcal{L}(\theta_t; \mathcal{B}_t)\|_{\Sigma_t}^2 + 2\eta_t^2 L (\text{tr}(\Sigma_t) + \beta_u) \sigma^2 + \mathcal{O}(\mu^2), \end{aligned}$$

where the second inequality is because of Lemma B.4 and the last inequality is because of the value of η_t .

Rearrange above equation and summing up it, we can obtain that

$$\begin{aligned} & \mathbb{E} \left[\sum_{t=1}^T \frac{\eta_t}{4} \|\nabla \mathcal{L}(\theta_t; \mathcal{B}_t)\|_{\Sigma_t}^2 \right] \leq \sum_{t=1}^T (\mathcal{L}(\theta_t; \mathcal{B}_t) - \mathcal{L}(\theta_{t+1}; \mathcal{B}_{t+1})) \\ & \quad + 2\eta_t^2 L (\text{tr}(\Sigma_t) + \beta_u) \sigma^2 + \mathcal{O}(T\mu^2) \\ & = \mathcal{L}(\theta_1; \mathcal{B}_1) - \mathcal{L}(\theta_{T+1}; \mathcal{B}_{T+1}) + 2\eta_t^2 L (\text{tr}(\Sigma_t) + \beta_u) \sigma^2 + \mathcal{O}(T\mu^2) \\ & \leq \mathcal{L}(\theta_1; \mathcal{B}_1) - \mathcal{L}(\theta_*; \mathcal{B}_*) + 2\eta_t^2 L (\text{tr}(\Sigma_t) + \beta_u) \sigma^2 + \mathcal{O}(T\mu^2). \end{aligned}$$

By taking $\theta_{\text{out}} = \theta_j$ with j uniformly sampled from $\{1, \dots, T\}$ and taking expectation, we can obtain that

$$\begin{aligned} & \mathbb{E} [\|\nabla \mathcal{L}(\theta_{\text{out}}; \mathcal{B})\|^2] = \frac{1}{T} \sum_{t=1}^T \|\nabla \mathcal{L}(\theta_t; \mathcal{B})\|^2 \leq \frac{1}{T\beta_\ell} \sum_{t=1}^T \|\nabla \mathcal{L}(\theta_t; \mathcal{B})\|_{\Sigma_t}^2 \\ & \leq \frac{4(\mathcal{L}(\theta_1; \mathcal{B}) - \mathcal{L}(\theta_*; \mathcal{B}))}{T\beta_\ell \eta} + \frac{8\eta L (\text{tr}(\Sigma_t) + \beta_u) \sigma^2}{T\beta_\ell} + \mathcal{O}(\mu^2) \\ & = \frac{32L (\text{tr}(\Sigma_t) + \beta_u) (\mathcal{L}(\theta_1; \mathcal{B}) - \mathcal{L}(\theta_*; \mathcal{B}))}{\sqrt{T}\beta_\ell} + \frac{\sigma^2}{T^{3/2}\beta_\ell} + \mathcal{O}(\mu^2), \end{aligned}$$

where the first inequality is because of the assumption that the diagonal entries of Σ_t is no less than β_ℓ , \square

Eq. (8) shows that once we choose the step size η properly, $\mathcal{L}(\theta_{t+1}; \mathcal{B}_{t+1})$ will be less than $\mathcal{L}(\theta_t; \mathcal{B}_t)$ in expectation up to some noises of order μ^2 . Specifically, if set $\eta = \frac{1}{8\sqrt{T}L(\max_t \text{tr}(\Sigma_t) + \beta_u)}$, Eq. (9) implies that we can find a solution θ_{out} such that $\mathbb{E} [\|\nabla \mathcal{L}(\theta_{\text{out}}; \mathcal{B})\|^2] \leq \epsilon^2$ in $\mathcal{O}(\epsilon^{-4})$ iterations. This rate matches the one of [15].

Lemma B.4. *We assume that Assumption B.2 and Assumption B.3 hold. Then, $g_\mu(\theta_t)$ defined in Eq. (7) has the following properties:*

$$\begin{aligned}\mathbb{E} [g_\mu(\theta_t)] &= \Sigma_t \nabla \mathcal{L}(\theta_t) + \mathcal{O}(\mu) \\ \mathbb{E} [\|g_\mu(\theta_t)\|^2] &\leq 4(\text{tr}(\Sigma_t) + \beta_u) \|\nabla \mathcal{L}(\theta_t)\|_{\Sigma_t}^2 \\ &\quad + 4\beta_u (\text{tr}(\Sigma_t) + \beta_u) \sigma^2 + \mathcal{O}(\mu^2).\end{aligned}$$

Proof. By the definition of $g_\mu(\theta_t)$, we have

$$\begin{aligned}g_\mu(\theta_t) &= \sum_{i=1}^b \frac{\mathcal{L}(\theta_t + \mu \Sigma_t^{1/2} u_i; \mathcal{B}_t) - \mathcal{L}(\theta_t - \mu \Sigma_t^{1/2} u_i; \mathcal{B}_t)}{2b\mu} \Sigma_t^{1/2} u_i \\ &= \sum_{i=1}^b \frac{2\mu \nabla^\top \mathcal{L}(\theta_t; \mathcal{B}_t) \Sigma_t^{1/2} u_i + \mathcal{O}(\mu^2)}{2b\mu} \Sigma_t^{1/2} u_i \\ &= \frac{1}{b} \sum_{i=1}^b \Sigma_t^{1/2} u_i u_i^\top \Sigma_t^{1/2} \nabla \mathcal{L}(\theta_t; \mathcal{B}_t) + \mathcal{O}(\mu).\end{aligned}$$

Thus, we can obtain that

$$\mathbb{E} [g_\mu(\theta_t)] = \Sigma_t \nabla \mathcal{L}(\theta_t; \mathcal{B}_t) + \mathcal{O}(\mu). \quad (12)$$

Moreover,

$$\begin{aligned}\mathbb{E} [\|g_\mu(\theta_t)\|^2] &= \mathbb{E} \left[\left\| \frac{1}{b} \sum_{i=1}^b \Sigma_t^{1/2} u_i u_i^\top \Sigma_t^{1/2} \nabla \mathcal{L}(\theta_t; \mathcal{B}_t) + \mathcal{O}(\mu) \right\|^2 \right] \\ &\leq 2\mathbb{E} \left[\left\| \frac{1}{b} \sum_{i=1}^b \Sigma_t^{1/2} u_i u_i^\top \Sigma_t^{1/2} \nabla \mathcal{L}(\theta_t; \mathcal{B}_t) \right\|^2 \right] + \mathcal{O}(\mu^2) \\ &\leq \frac{2}{b} \sum_{i=1}^b \mathbb{E} \left[\left\| \Sigma_t^{1/2} u_i u_i^\top \Sigma_t^{1/2} \nabla \mathcal{L}(\theta_t; \mathcal{B}_t) \right\|^2 \right] + \mathcal{O}(\mu^2) \\ &= 2\text{tr}(\Sigma_t) \cdot \nabla^\top \mathcal{L}(\theta_t; \mathcal{B}_t) \Sigma_t \nabla \mathcal{L}(\theta_t; \mathcal{B}_t) \\ &\quad + 2\nabla^\top \mathcal{L}(\theta_t; \mathcal{B}_t) \Sigma_t^2 \nabla \mathcal{L}(\theta_t; \mathcal{B}_t) + \mathcal{O}(\mu^2) \\ &\leq 2(\text{tr}(\Sigma_t) + \beta_u) \nabla^\top \mathcal{L}(\theta_t; \mathcal{B}_t) \Sigma_t \nabla \mathcal{L}(\theta_t; \mathcal{B}_t) + \mathcal{O}(\mu^2),\end{aligned}$$

where the last equality is because of Lemma B.5.

Finally, we have

$$\begin{aligned}\mathbb{E} [\nabla^\top \mathcal{L}(\theta_t; \mathcal{B}_t) \Sigma_t \nabla \mathcal{L}(\theta_t; \mathcal{B}_t)] &= \mathbb{E} [\|\nabla \mathcal{L}(\theta_t; \mathcal{B}_t)\|_{\Sigma_t}^2] \\ &\leq 2\mathbb{E} [\|\nabla \mathcal{L}(\theta_t)\|_{\Sigma_t}^2] + 2\mathbb{E} [\|\nabla \mathcal{L}(\theta_t; \mathcal{B}_t) - \nabla \mathcal{L}(\theta_t)\|_{\Sigma_t}^2] \\ &\leq 2\|\nabla \mathcal{L}(\theta_t)\|_{\Sigma_t}^2 + 2\beta_u \mathbb{E} [\|\nabla \mathcal{L}(\theta_t; \mathcal{B}_t) - \nabla \mathcal{L}(\theta_t)\|^2] \\ &\leq 2\|\nabla \mathcal{L}(\theta_t)\|_{\Sigma_t}^2 + 2\beta_u \sigma^2,\end{aligned}$$

where the second inequality is because of Assumption B.3 and the last inequality is because of Assumption B.2.

Therefore,

$$\mathbb{E} [\|g_\mu(\theta_t)\|^2] \leq 4(\text{tr}(\Sigma_t) + \beta_u) \|\nabla \mathcal{L}(\theta_t)\|_{\Sigma_t}^2 + 4\beta_u (\text{tr}(\Sigma_t) + \beta_u) \sigma^2.$$

□

Lemma B.5. [30] Let A and B be two symmetric matrices, and u obeys the Gaussian distribution, that is, $u \sim N(0, I_d)$. Define $z = u^\top A u \cdot u^\top B u$. The expectation of z is:

$$\mathbb{E}_u[z] = (\text{tr}A)(\text{tr}B) + 2\text{tr}(AB). \quad (13)$$

C Test Functions of the optimization trajectories

For better illustrating how HiZOO utilizes hessian to improve the convergence process, we choose below three test functions with heterogeneous curvatures across different parameters. In Figure 8, we provide the 2D convergence paths of three functions and the variation of their losses with respect to steps.

- Function (a)¹: $f(x, y) = 8(x - 1)^2(1.3x^2 + 2x + 1) + 0.5(y - 4)^2$
- Function (b): $f(x, y) = |x| + |y|$
- Function (c): $f(x, y) = 10000x^2 + y^2$

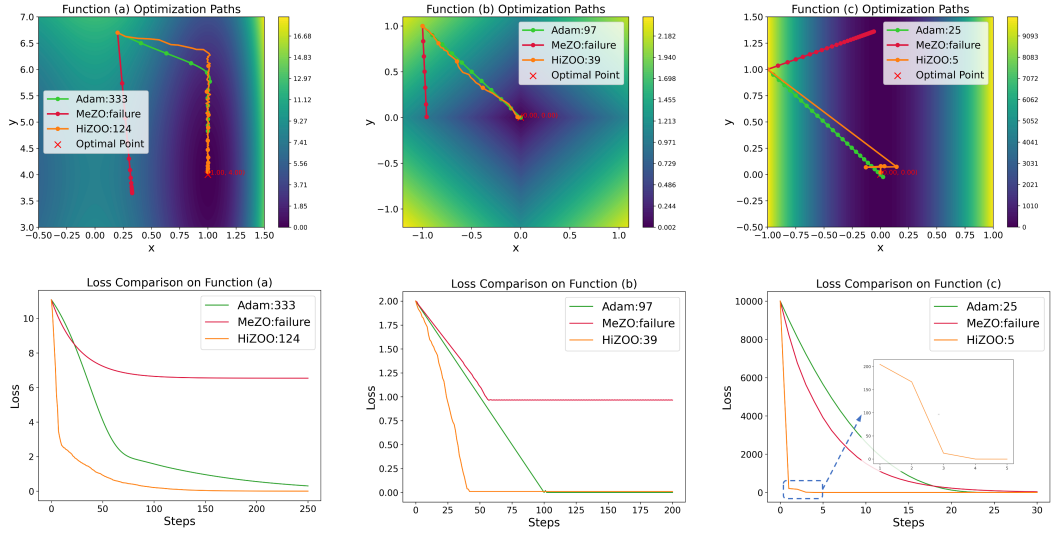


Figure 8: 2D trajectories of Adam, MeZO and HiZOO on 3 test functions. The upper figures are the 2D trajectories of gradient descent, and the bottom parts are the corresponding loss curves.

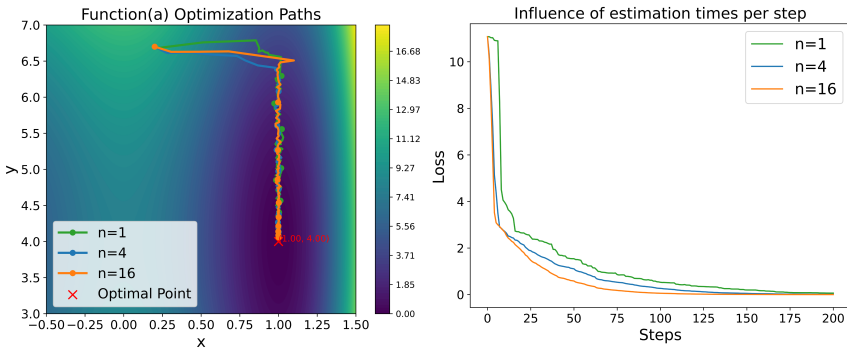


Figure 9: Influence of estimation times per step. (left) 2D trajectories of gradient descent; (right) Corresponding loss curves.

¹Function (a) is from [26].

Algorithm 2 HiZOO-multi

Require: parameters $\theta \in \mathbb{R}^d$, loss $L : \mathbb{R}^d \rightarrow \mathbb{R}$, step budget T , perturbation scale μ , batch size B , learning rate schedule η_t , smooth scale α_t , estimate times n , Hessian matrix Σ_0

- 1: **for** $t = 1, \dots, T$ **do**
- 2: seeds, projected_grads $\leftarrow []$
- 3: **for** $j = 1, \dots, n$ **do**
- 4: Sample batch $\mathcal{B} \subset \mathcal{D}$ and random seed s
- 5: $\ell \leftarrow \mathcal{L}(\theta; \mathcal{B})$
- 6: $\theta \leftarrow \text{PerturbParameters}(\theta, \mu, \Sigma_{t-1}^{1/2}, s)$
- 7: $\ell_+ \leftarrow \mathcal{L}(\theta; \mathcal{B})$
- 8: $\theta \leftarrow \text{PerturbParameters}(\theta, -2\mu, \Sigma_{t-1}^{1/2}, s)$
- 9: $\ell_- \leftarrow \mathcal{L}(\theta; \mathcal{B})$
- 10: $\theta \leftarrow \text{PerturbParameters}(\theta, \mu, \Sigma_{t-1}^{1/2}, s)$ ▷ Reset parameters before descent
- 11: $\Sigma'_t = \frac{1}{2\mu^2}(\ell_+ + \ell_- - 2\ell)(\Sigma_{t-1}^{-1/2}u_i u_i^\top \Sigma_{t-1}^{-1/2})$
- 12: $\Sigma_t^{-1} = (1 - \alpha_t)\Sigma_{t-1}^{-1} + \alpha_t |\text{diag}(\Sigma'_t)|$ ▷ Update Hessian matrix
- 13: projected_grad $\leftarrow (\ell_+ - \ell_-) * \Sigma_t^{1/2} / 2\mu$
- 14: projected_grads[j] \leftarrow projected_grad
- 15: seeds[j] $\leftarrow s$
- 16: **end for**
- 17: **end for**
- 18: **for** $j = 1, \dots, n$ **do**
- 19: Reset random number generator with seeds[j]
- 20: **for** $\theta_i \in \theta$ **do**
- 21: $u_i \sim \mathcal{N}(0, I_d)$
- 22: $\theta_i \leftarrow \theta_i - (\eta_t/n) * \text{projected_grads}[j] * u_i$ ▷ Avg grad for u_1, \dots, u_n
- 23: **end for**
- 24: **end for**
- 25: **function** PERTURBPARAMETER($\theta, \mu, \Sigma_t^{1/2}, s$)
- 26: Reset random number generator with seed s
- 27: **for** $\theta_i \in \theta$ **do**
- 28: $u_i \sim \mathcal{N}(0, I_d)$
- 29: $\theta_i \leftarrow \theta_i + \mu \Sigma_t^{1/2} u_i$ ▷ Modify parameters in place
- 30: **end for**
- 31: **return** θ
- 32: **end function**

D HiZOO Variants

D.1 HiZOO-multi

There is a rich history of transferring ideas from first order optimization to enhance ZO algorithms. Below, we highlight the variant of HiZOO: HiZOO-multi which can perform n estimation times per step efficiently as shown in Algorithm 2. We conducted experiments to explore the influence of estimation times n per step as shown in Figure 9. We can conclude that when n is larger, the estimation of diagonal Hessian is more accurate. It can decrease the variance of the estimated diagonal Hessian matrix during each step and thus reduce the overall training steps, but will cause much more computation per step meanwhile. So choosing an appropriate value of n is very important during the training.

D.2 HiZOO-L

Due to the storage of Hessian, HiZOO introduces extra memory cost, which is equal to the size of the model parameters. To address this limitations, we propose HiZOO-L, the low-rank implementation

Algorithm 3 HiZOO-L

Require: parameters $\theta \in \mathbb{R}^d$, loss $L : \mathbb{R}^d \rightarrow \mathbb{R}$, step budget T , perturbation scale μ , learning rate schedule η_t , smooth scale α_t , diagonal Hessian R_0, C_0

- 1: **for** $t = 1, \dots, T$ **do**
- 2: Sample batch $\mathcal{B} \subset \mathcal{D}$ and random seed s
- 3: $\ell \leftarrow \mathcal{L}(\theta; \mathcal{B})$
- 4: $\theta \leftarrow \text{PerturbParameters}(\theta, \mu, R_{t-1}, C_{t-1}, s)$
- 5: $\ell_+ \leftarrow \mathcal{L}(\theta; \mathcal{B})$
- 6: $\theta \leftarrow \text{PerturbParameters}(\theta, -2\mu, R_{t-1}, C_{t-1}, s)$
- 7: $\ell_- \leftarrow \mathcal{L}(\theta; \mathcal{B})$
- 8: $\theta \leftarrow \text{PerturbParameters}(\theta, \mu, R_{t-1}, C_{t-1}, s)$ ▷ Reset parameters before descent
- 9: $\hat{\Sigma}_{t-1}^{-1} = (R_{t-1} * C_{t-1}) / (1_n^\top * R_{t-1})$
- 10: $\hat{\Sigma}'_t = \frac{1}{2\mu^2}(\ell_+ + \ell_- - 2\ell)(\hat{\Sigma}_{t-1}^{-1/2} u_i u_i^\top \hat{\Sigma}_{t-1}^{-1/2})$
- 11: $R_t^{-1} = (1 - \alpha_t)R_{t-1}^{-1} + \alpha_t |\text{diag}(\hat{\Sigma}'_t)| * 1_m$
- 12: $C_t^{-1} = (1 - \alpha_t)C_{t-1}^{-1} + \alpha_t 1_n^\top * |\text{diag}(\hat{\Sigma}'_t)|$
- 13: projected_grad $\leftarrow (\ell_+ - \ell_-) * \hat{\Sigma}_t^{1/2} / 2\mu$
- 14: Reset random number generator with seed s ▷ For sampling u_i
- 15: **for** $\theta_i \in \theta$ **do**
- 16: Sample $u_i \sim \mathcal{N}(0, I_d)$
- 17: $\theta_i \leftarrow \theta_i - \eta_t * \text{projected_grad} * u_i$
- 18: **end for**
- 19: **end for**
- 20: **function** PERTURBPARAMETER(θ, μ, R_t, C_t, s) ▷ For sampling u_i
- 21: Reset random number generator with seed s
- 22: **for** $\theta_i \in \theta$ **do**
- 23: Sample $u_i \sim \mathcal{N}(0, I_d)$
- 24: $\hat{\Sigma}_t^{-1} = (R_t * C_t) / (1_n^\top * R_t)$
- 25: $\theta_i \leftarrow \theta_i + \mu \hat{\Sigma}_t^{1/2} u_i$ ▷ Modify parameters in place
- 26: **end for**
- 27: **return** θ
- 28: **end function**

for the storage of Hessian, motivated by Adafactor [41]. Details can be seen in Algorithm 2. We conduct lots of experiments to show the performance of HiZOO-L, as results shown in Figure 10.

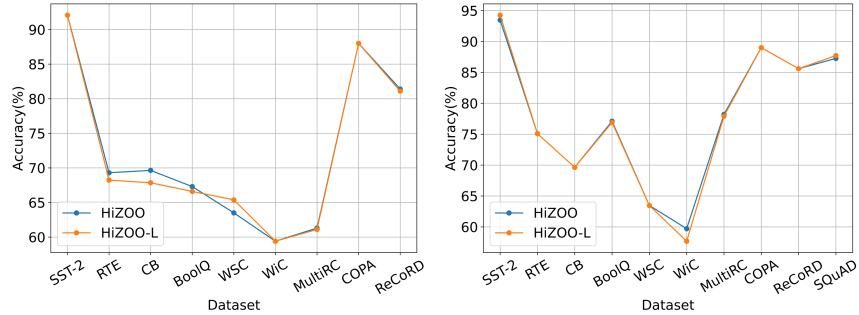


Figure 10: Accuracy comparison on OPT-13B (left) and Llama3 (right) between HiZOO and HiZOO-L.

Experiment	Hyperparameters	Values
HiZOO	Batch size	64
	Learning rate	{1e-7, 1e-6, 1e-5}
	μ	1e-3
	Weight Decay	0
HiZOO(prefix)	Batch size	64
	Learning rate	{1e-2, 5e-3, 1e-3}
	μ	1e-1
	Weight Decay	0
HiZOO(LoRA)	Batch size	64
	Learning rate	{1e-5, 5e-5, 1e-4}
	μ	1e-3
	Weight Decay	0.1
(r, α)		(8, 16)

Table 6: The hyperparameter grids used for RoBERTa-large experiments. HiZOO uses a constant learning rate schedule. All HiZOO experiments use 100K steps.

E Experiments on LLMs

E.1 Detailed Experiments on RoBERTa-large

We use the hyperparameters in Table 6 for HiZOO experiments on RoBERTa-large. Regarding learning rate scheduling and early stopping, we use constant learning rate for all HiZOO experiments.

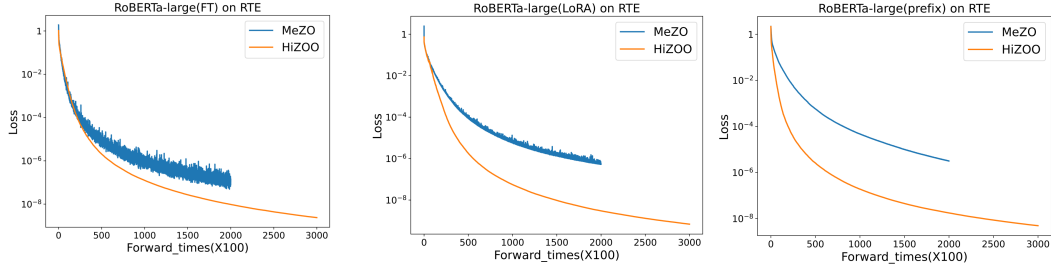


Figure 11: Loss curves on RoBERTa-large between MeZO and HiZOO.

Here we plot more loss curves to compare with MeZO. As shown in Figure 11, we can see that HiZOO can greatly accelerate the training process over MeZO, which verifies the robustness of HiZOO.

E.2 Detailed results on OPT

We use the hyperparameters in Table 7 for HiZOO experiments on OPT. We also provide the relative loss curves of fine-tuning OPT family in Figure 12.

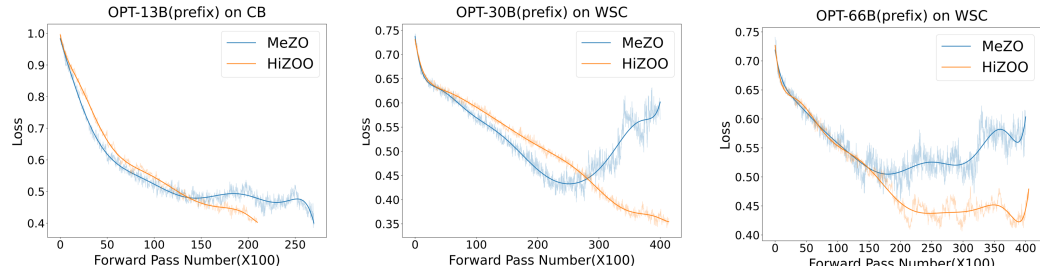


Figure 12: Loss curves on OPT between MeZO and HiZOO.

Experiment	Hyperparameters	Values
HiZOO	Batch size	16
	Learning rate	$\{1e-6, 5e-7, 1e-7\}$
	μ	$1e-3$
HiZOO(prefix)	Batch size	16
	Learning rate	$\{5e-2, 1e-2, 5e-3\}$
	μ	$1e-1$
HiZOO(LoRA)	# prefix tokens	5
	Batch size	16
	Learning rate	$\{1e-4, 5e-5, 1e-5\}$
FT with Adam	μ	$1e-2$
	(r, α)	$(8, 16)$
FT with Adam	Batch size	8
	Learning Rates	$\{1e-5, 5e-5, 8e-5\}$

Table 7: The hyperparameter grids used for OPT experiments. All weight decay is set to 0. HiZOO uses 20K steps and constant learning rates.

E.3 Detailed results on Phi-2 and Llama3

We provide several loss curves of fine-tuning Phi-2(2.7B) and Llama3(8B) in Figure 13 and Figure 14.

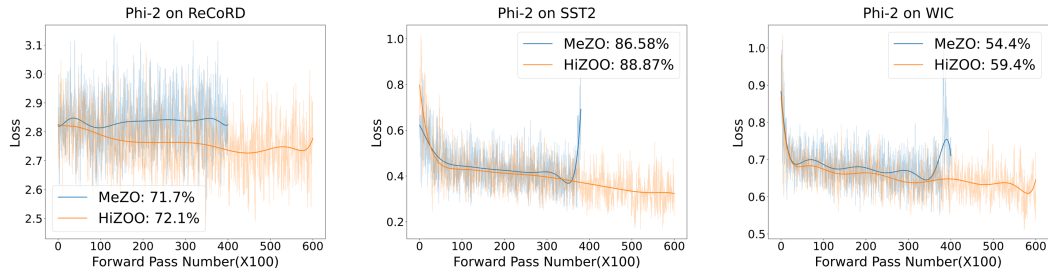


Figure 13: Loss curves on Phi-2 between MeZO and HiZOO.

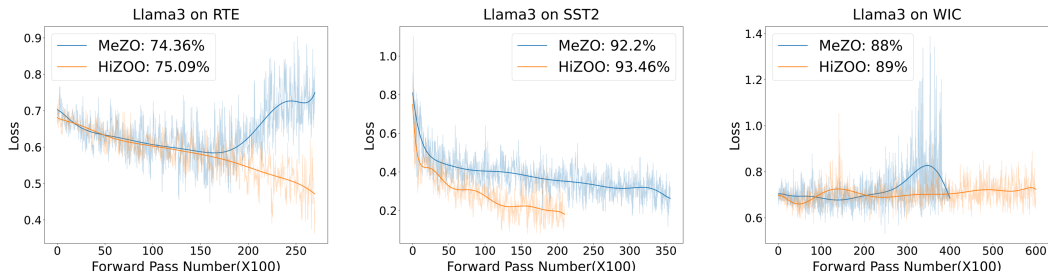


Figure 14: Loss curves on Llama3 between MeZO and HiZOO.

F Details about Memory Usage

Here we show the detailed numbers of memory profiling results Table 8. We did not turn on any advance memory-saving options, e.g., gradient checkpointing. We set the per-device batch size as 1 to test the minimum hardware requirement to run the model with specific optimization algorithms. We use Nvidia’s *nvidia – smi* command to monitor the GPU memory usage.

Method	zero-shot/MeZO(FT)	HiZOO(FT)	HiZOO-L(FT)	ICL	Adam(FT)
1.3B	1xA100 (4GB)	1xA100 (7GB)	1xA100 (4GB)	1xA100 (6GB)	1xA100 (27GB)
2.7B	1xA100 (7GB)	1xA100 (13GB)	1xA100 (8GB)	1xA100 (8GB)	1xA100 (55GB)
6.7B	1xA100 (14GB)	1xA100 (29GB)	1xA100 (15GB)	1xA100 (16GB)	2xA100 (156GB)
13B	1xA100 (26GB)	1xA100 (53GB)	1xA100 (29GB)	1xA100 (29GB)	4xA100 (316GB)
30B	1xA100 (58GB)	2xA100 (118GB)	1xA100 (64GB)	1xA100 (62GB)	8xA100 (633GB)
66B	2xA100 (128GB)	3xA100 (246GB)	2xA100 (140GB)	2xA100 (134GB)	16xA100

Table 8: Memory usage on the MultiRC (average tokens=400) dataset. Results of ICL and full-parameter tuning are from MeZO[32].

G Details about Wallclock Time Efficiency

In this section, we measure the wallclock time efficiency of HiZOO compared to MeZO and full-parameter fine-tuning (FT) with respect to different model sizes. Due to the lack of NV-Link connectivity in our A100 GPUs, we selected models that can be fully fine-tuned on a single A100 GPU for comparison. As shown in Table 9, HiZOO exhibits a longer per-step duration compared to MeZO, within a 50% margin. This result indicates that the primary overhead in hierarchical optimization methods lies in the forward propagation process. Given that HiZOO involves an additional forward pass compared to MeZO, the time per step increases by approximately 1.4 to 1.5 times.

In conclusion, the speedup factors derived from the forward pass step used in our comparisons between HiZOO and MeZO reflect the actual wallclock time efficiency improvements accurately.

Model	RoBERTa-large(350M)	Phi-2(2.7B)	Llama3(8B)	OPT(13B)
MeZO	0.2092s(BS=64)	0.3011s(BS=16)	0.7471s(BS=16)	1.1108s(BS=16)
HiZOO	0.3023s(BS=64)	0.4486s(BS=16)	1.1090s(BS=16)	1.5225s(BS=16)
HiZOO-L	0.3193s(BS=64)	0.4851s(BS=16)	1.1996s(BS=16)	1.6422s(BS=16)

Table 9: Wallclock time per step between MeZO and HiZOO. The increase in wallclock time per step for HiZOO compared to MeZO is less than 1.5 times across different model sizes. To avoid introducing additional overheads such as inter-GPU communication, results are measured on the same dataset (SST-2) and GPUs (80GB A100), with each result averaged over 100 steps. "BS" refers to batch size. For the relatively smaller RoBERTa-large model, we used a BS=64, while for models larger than 1B parameters, we used a BS=16.

H Details about Ablation Experiments

H.1 Influence of Smooth Scale α_t

We conducted experiments on SST-2, SST-5, MNLI datasets when fine-tuning RoBERTa-large to research the influence of smooth scale α_t . Figure 15 shows that the value of α_t mainly affects the convergence speed of the model. Additionally, the best value of α_t will vary between different datasets.

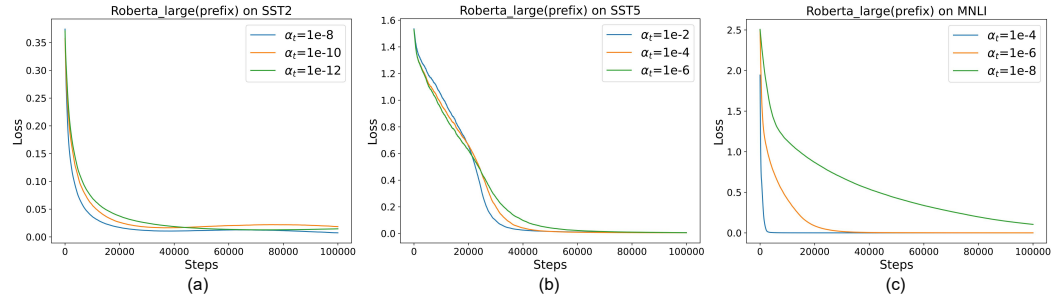


Figure 15: More experiments on influence of the value of Smooth scale α_t on RoBERTa.

H.2 Experiments about Omitting $[-\Sigma^{-1}]$ term in Eq. (5)

We conducted experiments on SST-2 datasets using three methods to fine-tune RoBERTa-large to compare the difference between with $[-\Sigma^{-1}]$ term and without this term. Figure 16 shows that this term can make negligible influence.

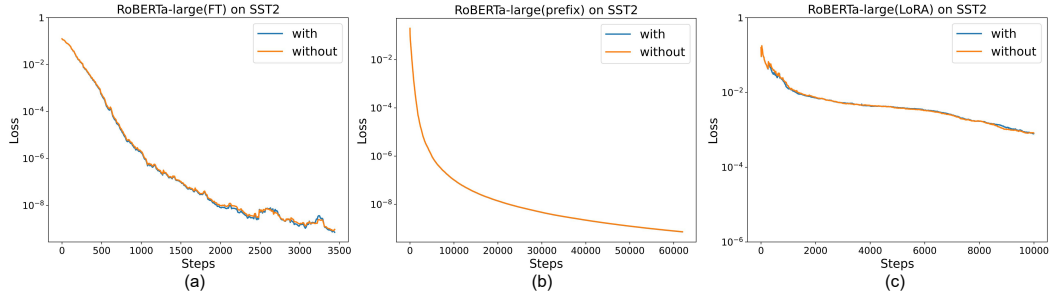


Figure 16: Experiment about the error generate by omitting the $[-\Sigma^{-1}]$ term in Eq (5). 'with' means holding the term and 'without' means omitting the term.